Optica Applicata, Vol. XLII, No. 3, 2012
DOI: 10.5277/oa120315

Modeling of a high performance Mach–Zehnder interferometer all optical switch

GHANSHYAM SINGH*, VIJAY JANYANI, R.P. YADAV

Department of Electronics and Communication Engineering,
Malaviya National Institute of Technology Jaipur-302017, India

*Corresponding author: gschoudhary75@gmail.com

In this work, a detailed performance analysis for a Mach–Zehnder interferometer (MZI) optical switch with a channel profile of titanium-indiffused lithium niobate ($Ti:LiNbO_3$) is presented. The concept of diffusion process controlled modeling has been used to design and optimize its performance. Impacts of Ti-strip thickness on the power imbalance of first 3-dB coupler and crosstalk (CT) levels at the end of the interferometric arms are defined and calculated. Transition losses in the curved waveguides of the structure are maintained at low levels by selecting low less bend structures to increase overall performance of the switch. The best CT levels of –41.73 dB for cross state and –32.69 dB for bar state at 1.3 μm wavelength have been achieved. While at 1.55 μm wavelength, a CT of –41.73 dB for cross state and –33.99 dB for bar state have been observed. The switch designed was found to operate best at 7.25 V and 8.25 V for test wavelengths of 1.3 μm and 1.55 μm, respectively. The computed results for its performance are better as compared to the present published data.

Keywords: MZI-structure, $Ti:LiNbO_3$, process control parameters, switch losses, crosstalk levels.

1. Introduction

Among all available topologies, MZI structures are most efficient to convert a phase modulation into an intensity modulation. These structures are often used to build optical modulators, splitters, switches [1–9], logic gates and Boolean function generators [10–14] with the use of electro-optic (EO) or thermo-optic (TO) effects. Utilizing the EO-effects, the symmetric MZI structure has been preferred to design flexible and high-speed optical switches with low driving power requirements for the shortest switching window. This structure has been preferred to realize optical switches with polymers [2, 3], $LiNbO_3$ [6, 7] and III–V semiconductors and their composites [8, 9], silica [15], photonic crystals [16], *etc*. MZI structure can easily be extended to perform various optical logical and Boolean operations with use of single or parallel semiconductor optical amplifiers (SOAs) in its arms or using multiple and sort waveguides at the interferometric arms [17–20]. Due to large EO coefficients, lithium niobate (LN) is a suitable back plane for MZI-based modulators/switches and possesses stable performance parameters (optical loss, crosstalk, *etc*.), even for inputs with different optical power levels [21].

Lithium niobate waveguides have been fabricated using titanium-indiffusion, which increases refraction indices of the selected diffused area of the waveguides and allows both polarized modes (TE and TM) to propagate [22]. This paper reviews the design and performance of a compact 2×2 symmetric MZI switch, based on a channel profile of Ti:$LiNbO_3$ (Ti-LN). The effect of Ti-strip thickness on the indiffusion process has been used to calculate the power imbalance in the structure and its subsequent impact on the CT levels at end facet of the interferometric arms. The effect of various indiffusion process parameters, *e.g*., dopant strip thickness, lateral and vertical diffusion length on the insertion loss has been taken care of, to reduce the switch losses. The switch performance has been evaluated for its operations for low attenuation optical windows with least possible driving voltage and minimum losses during switching action.

2. Switching phenomena in MZI-structures

The MZI switch, as shown in Fig. 1, cycles between the bar state, where most of the light appears in the waveguide on the same side as the input, and the cross state, where most of the light moves to the waveguide on the other side [1].

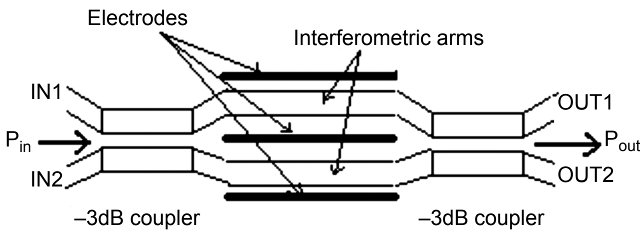

Fig. 1. Electro-optic MZI switch with equal interferometric arm lengths [1].

A conventional EO-effect based 2×2 MZI switch consists of two interferometric arms of equal length connected between two 3dB-couplers. These arms are placed far enough from each other to avoid evanescent coupling between them. The first coupler is used to split the light evenly into two beams, which when passed through the interferometric arms experiences a net phase change of $2\Delta\phi$. This phase difference is due to a push–pull effect caused by the field applied in opposite directions through the waveguides under the electrodes [23]. This causes the light to constructively or destructively interfere at the output depending on the field (phase) applied.

T a b l e 1. Comparison of EO-MZI switches.

Material	Design specifications	Test wavelength	Switching voltage	CT	Insertion loss IL	Others	Ref.
Polymer	Elect. length: 5 mm	1.55 μm	±0.925 V	–30 dB	≤ 5.91 dB	–	[2]
Polymer	Overall length: 4 cm Elect. length: 1.5 cm	1.3 μm	15 V	From –22 to –27 dB	From 9 to 10 dB	Propagation loss 1–1.25 dB/cm	[3]
IPC-E/polysulfone	UV15 (lower) and NOA61 (upper) cladding layers	1.55 μm	–	≥ –25 dB	≤ –1.8 dB	–	[4]
Si	Area: 400 nm×340 nm, Modulation arm: 1 mm	–	–	±28 dB	–	Extinction ratio 40 dB	[5]
Ti-LN	Elect. length: 10 mm, Thickness: 4 μm	1.3 μm	12 V	–	–	–	[6]
Ti-LN	Elect. length: 10 mm, Thickness: 4 μm	1.3 μm	8 V	–	From 0.06 to0.70 dB	Extinction ratio 11.9–22.94	[7]
InP	Waveguide width: 3 μm, use of phase shifter	1.5–1.6 μm	7.5–9 V	From –20 to –30 dB	≤ 2 dB	Total on-chip losses: 3–9 dB	[8]
GaAs–GaAlAs	Overall length: 1.4 cm, use of carrier-injection method, elect. length is 500 μm with a 35 μm spacing between each other	1.55 μm	1.35–1.48 V	–	2 dB with prop. loss: 0.5 dB/cm	Extinction ratio ≥ 20 dB Power consumption ≤ 66 mW	[9]

Accumulation of a phase difference between the two arms causes the recombined light to interfere according to the following equation [24]

$$\frac{P_{\text{out}}}{P_{\text{in}}} = \frac{1 + \cos(\Delta\phi)}{2} \tag{1}$$

Various materials have been used with their EO properties to design and implement MZI-based optical switches for two most popular optical windows, *i.e.*, 1.3 μm and 1.55 μm. Table 1 gives a comparison of some EO-switches based on MZI structure, reported in the last decade.

3. Lithium niobate: a perfect crystal for photonic switching

Lithium niobate is a colorless, ferroelectric, water insoluble and an extremely versatile nonlinear crystal material suitable for a variety of applications. It exhibits a large electro-optic (EO), acousto-optic (AO), thermo-optic (TO) effects [25, 26], which makes it suitable in modern optics as an integrated optical element. With unique EO properties of LN, it has been used to grow large wafer substrates that can exhibit small dielectric constant and can be used for fast device responses with low power consumption. In this crystal, EO-effect takes place linearly, *i.e.*, the size of perturbation to the refractive index is directly proportional to the strength of the local electrostatic field [22]. Also it is anisotropic in nature; therefore its physical properties such as absorbance, refractive index, density, *etc*., are directionally dependent, *i.e.*, having difference in their values when measured along different axis. Distribution of refractive index in LN along the three axes (X, Y, Z) can be represented in indicatrix or ellipsoid form as follows [22]

$$\frac{X^2}{n_o^2} + \frac{Y^2}{n_o^2} + \frac{Z^2}{n_e^2} = 1 \tag{2}$$

where n_o, n_e are the ordinary and extraordinary refractive indices, respectively. In our work, the waveguides, which have been designed with Ti-LN, are employed with metallic electrodes to serve the purpose of applying the electric field. The calculation of an electric field of the coplanar electrodes is based on [27]. Under the influence of electric field the index ellipsoid is deformed in space and in different cases of the crystal cut, propagation directions, polarization, and the electric field direction, refractive index change can be calculated with the help of different EO-coefficients r_{ij} accordingly. If voltage is then applied along the z-axis of the crystal, the new index ellipsoid can be expressed as follows [22, 28]

$$\left(\frac{1}{n_o^2} + r_{13}E_z\right)x^2 + \left(\frac{1}{n_o^2} + r_{13}E_z\right)y^2 + \left(\frac{1}{n_e^2} + r_{33}E_z\right)z^2 = 1 \tag{3}$$

The change in the corresponding refractive index can be approximated as [18]

$$n_i' = n_i + \frac{n_i^3}{2}\left(r_H E_H + r_V E_V\right) \tag{4}$$

where i denotes either ordinary or extraordinary refractive index and E_H, E_V, r_H, and r_V are the electric fields and corresponding electro-optic coefficients in horizontal and vertical directions. In our case, LN crystal coordinate system is different from the device layout coordinate system. The crystal cut direction is conventionally assumed as perpendicular to the crystal wafer surface. The optical fields, being the principal electrical component of the electromagnetic field, can oscillate horizontally (TE polarization) or vertically (TM polarization) to the surface. With the help of appropriate electro-optic or Pockels coefficient matrix [29] values, calculation of refractive index difference has been done.

4. Ti-indiffusion in lithium niobate

Titanium indiffusion with LN serves the purpose of perfect electro-optic behavior to achieve optical switching. The indiffusion process is carried out by placing a Ti-strip of fixed thickness and width onto LN substrate followed by heating within defined process environment. After the process, the titanium ions are able to penetrate the host substrate and form a graded index waveguide of defined pattern. The following concepts of Ti-indiffusion process within LN substrate are mainly taken from *Technical Background and Tutorials*, ver. 8, Optiwave Inc. 2006 [22]. The bell-shaped refractive index distribution of the graded waveguide in the lateral and in-depth directions can be characterized by diffusion lengths or, as an alternative, by diffusion constants, diffusion temperature and a diffusion temperature coefficient. This graded refractive index profile can be characterized by the following equation

$$n_i(\lambda, x, y) = n_i^{(o)}(\lambda) + \Delta n_i(\lambda, x, y), \qquad i = o, e \tag{5}$$

where $n_i^{(o)}$ is the bulk crystal index, Δn_i is the diffusion induced index change, and the subscripts o and e are ordinary and extraordinary index distributions. The bell-shaped dopant concentration profile can be described as follows,

$$c(x, y) = c_o\left\{\mathrm{erf}\left[\frac{w}{2D_H}\left(1 + \frac{2x}{w}\right)\right] + \mathrm{erf}\left[\frac{w}{2D_H}\left(1 - \frac{2x}{w}\right)\right]\right\}\exp\left(-\frac{y^2}{D_V^2}\right) \tag{6}$$

The profile parameters include the profile constant c_o, the dopant stripe width before diffusion w, the horizontal (lateral) diffusion length D_H, and the vertical (in depth) diffusion length D_V. The horizontal and vertical diffusion lengths are functions of the diffusion time t and the diffusion temperature T and can be determined as

$$D_H = 2\sqrt{tD_{OH}\exp\left(-\frac{T_0}{T}\right)} \tag{7}$$

$$D_V = 2\sqrt{tD_{OV}\exp\left(-\frac{T_0}{T}\right)} \tag{8}$$

The temperature coefficient T_0 and the diffusion constants in horizontal and vertical directions, D_{OH}, D_{OV} are specific to the Ti-LN. The concentration profile constant is a function of the dopant (Ti) stripe thickness before diffusion t_s, the dopant constant c_m, and the vertical diffusion length D_V

$$c_0 = \frac{t_s c_m}{D_V\sqrt{\pi}} \tag{9}$$

The dopant constant c_m is a material parameter determined by the dopant density ρ, atomic weight M_{at} and Avogadro's number N_A.

5. Design and analysis of EO-effect based 2×2 MZI switch

5.1. Design steps

For our design, we assume that the MZI structure as shown in Fig. 2 is created on a z-cut LN substrate with propagation direction along y-axis. The channel waveguides are created by indiffusion of Ti in LN substrate. The device is designed on an OptiBPM layout platform and the initial RI profile of the guiding structure (xy-slice) is verified using 2D and 3D simulators. The dimensions of various sections and other design specifications are set as in Tab.2. The wafer has the same refractive index as that of LN along with 3D wafer properties including air as cladding material with a thickness

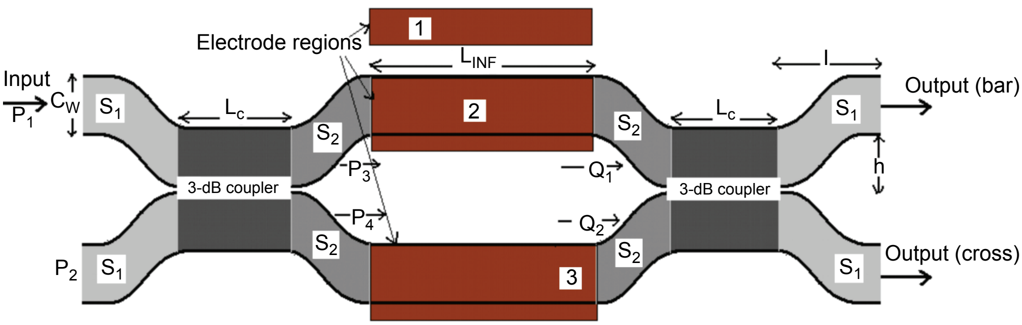

Fig. 2. Proposed MZI switch with various labeled regions and input and output power definitions of first coupler (3-dB splitter) and second coupler (3-dB combiner).

T a b l e 2. Design specifications for MZI switch proposed.

Channel waveguide and diffusion process specifications	
Wafer dimension	L = 33 mm, W = 8.0 μm, thickness = 0.1 mm
Substrate material	$LiNbO_3$ (thickness: 0.1 mm)
Cladding material	Air (thickness: 0.02 mm)
Channel profile	Ti-indiffused LN
Substrate (LN) specifications	
Refractive index	$n_o = 2.211$, $n_e = 2.138$
EO-coefficients (10^{-12} m/V)	$r_{33} = 30.8$, $r_{13} = 8.6$, $r_{51} = 28$, $r_{22} = 3.5$
Range of Ti-stripe thickness	0.045–0.095 μm
Dopant constant	5.67×10^{22}
Sectional dimensions	
Length of coupling section L_c	3.25 mm
Length of Interferometric arms L_{INF}	10 mm
S-bend S_1: trans. length l	5.75 mm
S-bend S_1: lateral offset h	12.75 mm
S-bend S_2: trans. length l	2.5 mm
S-bend S_2: lateral offset h	8.75 mm

T a b l e 3. Specification of the designed device.

Wafer and guiding channel	
Device dimensions	L = 33 mm, W = 0.01 mm
Crystal cut direction	z-cut; propagation direction: y
Thickness	Substrate (LN) = 10 μm, cladding (air) = 2 μm
Substrate (LN) specifications	
Refractive index*	$n_o = 2.211$, $n_e = 2.138$
EO-coefficients (10^{-12} m/V)	$r_{33} = 30.8$, $r_{13} = 8.6$, $r_{51} = 28$, $r_{22} = 3.5$
Ti-indiffusion process specifications	
Dopant constant	5.67×10^{22} per cm^2
Diffusion time	2.5 hour
Dispersion factor*	$d_o = 0.7701$, $d_e = 0.8968$
Distribution constant*	$F_o = 1.3\times10^{-25}$ cm^{-3}, $F_e = 1.2\times10^{-23}$ cm^{-3}
Distribution factor*	$\gamma_o = 0.5$, $\gamma_e = 0.5$
Diffusion constant*	$D_{OV} = D_{OH} = 0.023$ cm^2/s
Diffusion temperature	1050 °C
Temperature coefficient T_o	30300 K
Variable parameters	
Dopant (Ti) stripe thickness t_s	0.045 μm–0.095 μm
Lateral diffusion length D_H	2.6 μm–4.6 μm
Diffusion length in depth D_V	2.0 μm–4.5 μm

*Subscript o denotes ordinary and e represents extraordinary values.

of 2 μm and LN as substrate with a thickness of 10 μm. The guiding channel with a width of 8.0 μm in the form of MZI structure is created by Ti-indiffusion within LN substrate.

Using Ti-indiffusion onto LN, a guiding channel with a bell-shaped refractive index profile is obtained by placing a few μm thick t_s Ti-strip and then setting the process temperature and time at 1050 °C and 2.5 hrs, respectively. The initial design parameters set for the substrate and Ti-indiffusion process to form Ti-LN channel are depicted in Tab. 3. Ti doping in the LN substrate changes its refractive indices, which is a function of parameters like Ti-strip thickness t_s, lateral diffusion length D_H, vertical diffusion length D_V and other process parameters. With controlled indiffusion process, *i.e.*, by controlling the aforementioned process parameters, various loss levels of the device have been minimized. Ti-strip thickness t_s has been varied to determine the amount of Ti indiffusion in the host and to select the best value to optimize the device performance.

A controlled modulating electric field within the structure is provided by defining suitable electrode regions in the subsequent step. To isolate the guiding layers and electrode regions, a dielectric buffer layer of SiO_2 (thickness = 0.3 μm, refractive index = 1.47) with equal horizontal and vertical permittivity is placed above the guiding channel layer. On the top of this buffer layer, electrodes of equal length and thickness (10 mm and 4.0 μm, respectively) with a spacing of 6.0 μm between each other are placed as shown in Fig. 3. The width of electrodes 1, 2 and 3 are 50 μm, 26 μm and 50 μm, respectively. The length is carefully chosen to be 10 mm, so as to produce equal and maximum overlapping of optical and electrical field by covering the whole part of interferometric arms.

5.2. Performance analysis and results

The device performance is checked by performing 2D isotropic simulation using paraxial beam propagation method with finite difference engine scheme parameter

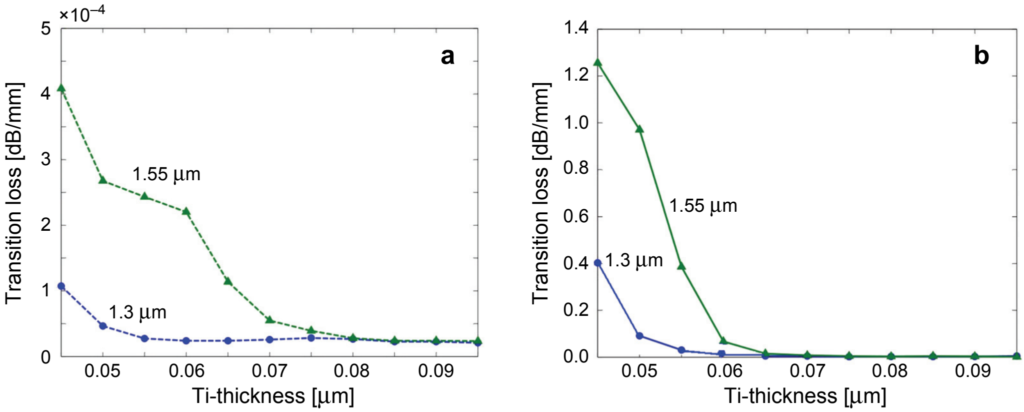

Fig. 3. Loss variation vs. Ti-thickness t_s for straight waveguides (**a**) and curved (*s*-bend) waveguides (**b**).

of 0.5, propagation step of 1.3 and transparent boundary conditions [22]. The global data is set with refractive index MODAL and TM polarized test signals at wavelengths of 1.3 μm and 1.55 μm are considered. Initially, the transition losses for straight and curved (*s*-bends) waveguides were calculated by varying t_s in the range of 0.045–0.095 μm. It was observed that these losses can be kept at negligible levels (which are $\leq 0.4\times10^{-3}$ dB/mm for straight and ≤ 0.003 dB for curved waveguides), if the value for t_s is chosen as ≥ 0.050 μm for test wavelength of 1.3 μm and ≥ 0.065 μm for 1.55 μm operation as shown by plotted results of Figs. 3**a** and 3**b**.

Further, to observe the imbalance and their impact on the CT levels generated at the end facet of interferometric arms with respect to variations in t_s, the power levels at the end of the 1st coupler were monitored as shown in Fig. 3. These parameters are calculated using the following definitions [8].

Imbalance at the output of splitter:

$$U = 10\log\left(\frac{P_3}{P_4}\right) \tag{10}$$

CT at the end of interferometric arms:

$$\mathrm{CT_{INF}} = 10\log\frac{\left[\left(\frac{Q_1}{2}\right)^{1/2} - \left(\frac{Q_2}{2}\right)^{1/2}\right]^2}{\left[\left(\frac{Q_1}{2}\right)^{1/2} + \left(\frac{Q_2}{2}\right)^{1/2}\right]^2} \tag{11}$$

Further, Q_1 and Q_2 are power levels at the end of interferometric arms and are expressed as [8]

$$Q_1 = \frac{1}{10^{U/10} + 1} \quad \text{and} \quad Q_2 = 1 - Q_1 \tag{12}$$

Using Equations (10)–(12), it has been found that the CT levels at the end of the interferometric arms tend to become worse with an increase in power imbalance, as shown in Fig. 4. These CT levels at the end of the interferometric arms tend to vary almost irrespective of test wavelengths. The best CT levels at the end of interferometric arms are obtained for t_s of 0.054 μm, which is −43.75 dB at 1.3 μm test wavelength and −42.25 dB at 1.55 μm test wavelength, while the t_s before indiffusion process was taken as 0.0825 μm.

The switch, while in cross state exhibited a minimum insertion loss (IL), excess loss (EL) and CT of the order of 0.018 dB, 0.017 dB, −41.73 dB, respectively for operating wavelength of 1.3 μm. While for the test wavelength of 1.55 μm with t_s of 0.0825 μm, the values of IL, EL and CT are of the order of 0.006 dB, 0.005 dB and

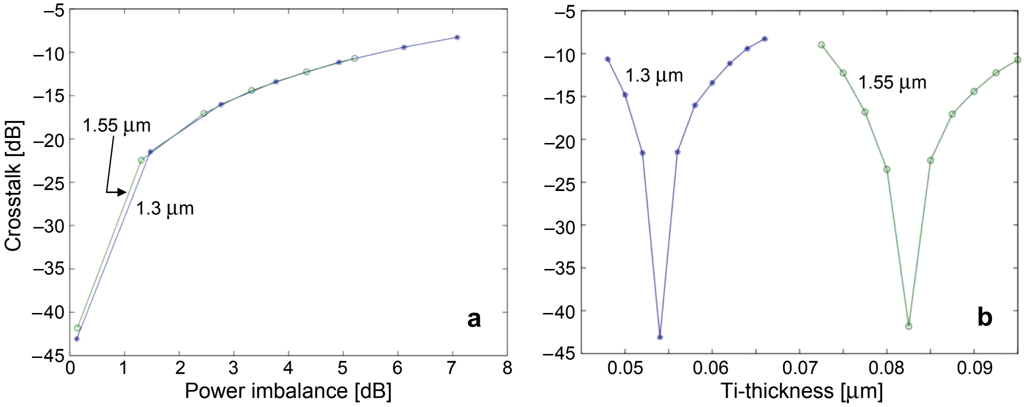

Fig. 4. Calculated CT levels due to variation in power imbalance (**a**) and variations in t_s (**b**); switch state: cross.

–39.60 dB, respectively. The extinction ratio (ER) is observed higher than 40 dB for either case of test wavelength with these values of t_s. Further, indiffusion process parameters such as lateral and vertical diffusion lengths (D_H and D_V) were varied in order to find their optimum values for our design case. The switch losses and ER were found to be more sensitive to variation in the D_H as compared to D_V. We also found that, with D_H at 3.5 µm and D_V at 4.5 µm, the switch operation proved to be more stable and possess better performance parameters for the design specifications and dimensions considered. Finally, the switch was forced to go into its bar state with EO-effect, by applying voltage across the electrodes in the range 6.0–9.0 V and corresponding performance parameters were calculated.

Figure 5 shows the CT variation in response to the applied voltages, with the switch operating in its bar state. From these plots, it is clear that the switching performance

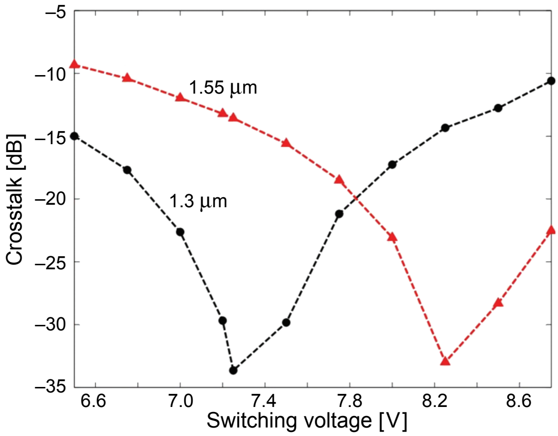

Fig. 5. Calculated CT levels of the switch (in bar state) as a function of switching voltages for $\lambda = 1.3$ µm (with $t_s = 0.054$ µm) and 1.55 µm (with $t_s = 0.0825$ µm).

is at its best at 7.25 V and at 8.25 V, for a test wavelength at 1.3 μm and 1.55 μm wavelength, respectively. Also, with these test wavelengths, the switch maintains a CT level better than –30 dB. Meanwhile, for most cases, the ER of more than 38 dB for cross state and 40 dB for bar state at both test wavelengths has been observed. In the worst case polarization dependent loss (PDL) was found to be less than 0.3 dB and 0.4 dB for light inputs at the wavelengths of 1.55 μm and 1.3 μm, respectively. In the bar state, the best CT level of –32.69 dB and –33.99 dB at test wavelengths of 1.3 μm and 1.55 μm has also been achieved.

6. Conclusions

A compact, high performance 2×2 MZI-switching structure is proposed with a channel profile of Ti-indiffused lithium niobate. The effect of Ti-strip thickness on the power imbalance of first 3-dB coupler and crosstalk levels at the end of the interferometric arms are calculated and plotted. The best CT levels of −41.73 dB for cross state and –32.69 dB for bar state at 1.3 μm wavelength have been achieved. While at 1.55 μm wavelength, a CT of −41.73 dB for cross state and –33.99 dB for bar state have been achieved. With the measured results, we conclude that power imbalance in the structure and subsequent generation of CT will have a great impact on its working, while using it as a optical switch, modulator, *etc*. These parameters can be improved further with more precise and controlled Ti-indiffusion process within the waveguide material. With this work, we are able to demonstrate an MZI switch built with Ti-LN guiding channel with negligible losses; however, the scope lies in reducing the CT levels further and using this structure in modeling Boolean logical units and multiplexers with integration of semiconductor optical amplifiers in its interferometric arms [30–32].

Acknowledgements – The authors gratefully acknowledges the Centre for International Mobility (CIMO), Government of Finland for awarding the CIMO Fellowship to visit and work with Nanofabrication facilities, Department of Physics and Mathematics, University of Eastern Finland, Joensuu (Finland).

References

[1] Papadimitriou G.I., Papazoglou C., Pomportsis A.S., *Optical Switching*, Wiley Series in Microwave and Optical Engineering, Wiley, 2007.

[2] Zheng C.-T., Ma C.-S., Yan X., Zhang D.-M., *Design of a spectrum-expanded polymer MZI electro-optic switch using two-phase generating couplers*, Applied Physics B: Lasers and Optics **102**(4), 2011, pp. 831–840.

[3] Wol-Yon Hwang, Min-Cheol Oh, Hyang-Mok Lee, Heuk Park, Jang-Joo Kim, *Polymeric 2×2 electrooptic switch consisting of asymmetric Y junctions and Mach–Zehnder interferometer*, IEEE Photonics Technology Letters **9**(6), 1997, pp. 761–763.

[4] Li H.P., Liao J.K., Tang X.G., Lu R.G., Liu Y.Z., *2×2 polymeric electro-optic MZI switch using multimode interference couplers*, Proceedings of SPIE **7509**, 2009, article 75090X.

[5] Xu Xue-Jun, Chen Shao-Wu, Xu Hai-Hua, Sun Yang, Yu Yu-De, Yu Jin-Zhong, Wang Qi-Ming, *High-speed 2×2 silicon-based electro-optic switch with nanosecond switch time*, Chinese Physics B **18**(9), 2009, pp. 3900–3904.

[6] YAHYA E.H.M, *Mach–Zehnder Interferometer*, M. Tech. Thesis, Faculty of Electrical Engineering, University of Technology Malaysia, April 2007.
[7] RAHMAN M.S.A., SHAKTUR K.M., MOHAMMAD R., *Analytical and simulation of new electro-optic 3×3 switch using a Ti:LiNbO$_3$ waveguide medium*, 2010 International Conference on Photonics (ICP), 2010, pp. 1–5.
[8] MAAT D.H.P., *InP-Based Integrated MZI Switches for Optical Communication*, PhD Thesis, Department of Applied Physics, Delft University of Technology, Delft, The Netherlands, 9 April, 2001.
[9] SHAOCHUN CAO, LIPING SUN, SAVOIE M., *2×2 MMI–MZI GaAs–GaAlAs carrier-injection optical switch*, 2010 IEEE Photonics Society Summer Topical Meeting Series, 2010, pp. 207–208.
[10] HOUBAVLIS T., ZOIROS K.E., KANELLOS G., TSEKREKOS C., *Performance analysis of ultrafast all-optical Boolean XOR gate using semiconductor optical amplifier-based Mach–Zehnder interferometer*, Optics Communications **232**(1–6), 2004, pp. 179–199.
[11] MIN ZHANG, YONGPENG ZHAO, LING WANG, JIAN WANG, PEIDA YE, *Design and analysis of all-optical XOR gate using SOA-based Mach–Zehnder interferometer*, Optics Communications **223**(4–6), 2003, pp. 301–308.
[12] CHEN H., ZHU G., WANG Q., JAQUES J., LEUTHOLD J., PICCIRILLI A.B., DUTTA N.K., *All-optical logic XOR using differential scheme and Mach–Zehnder interferometer*, Electronics Letters **38**(21), 2002, pp. 1271–1273.
[13] DIMITRIADOU E., ZOIROS K.E., *On the design of ultrafast all-optical NOT gate using quantum--dot semiconductor optical amplifier-based Mach–Zehnder interferometer*, Optics and Laser Technology **44**(3), 2012, pp. 600–607.
[14] CHATTOPADHYAY T., *All-optical modified Fredkin gate*, IEEE Journal of Selected Topics in Quantum Electronics **18**(2), 2012, pp. 585–592.
[15] SUZUKI K., YAMADA T., MORIWAKI O., TAKAHASHI H., OKUNO M., *Polarization-insensitive MZI switch composed of an LN phase shifter array and silica-based PLC-integrated polarization beam splitter*, Conference on Optical Fiber communication/National Fiber Optic Engineers Conference, 2008, OFC/NFOEC 2008, pp. 1–3.
[16] HAN TAE YONG, HYUN-SHIK LEE, EL-HANG LEE, *Design of compact silicon optical modulator using photonic crystal MZI structure*, 2008 5th IEEE International Conference on Group IV Photonics, 2008, pp. 308–310.
[17] YAW-DONG WU, *All-optical logic gates by using multibranch waveguide structure with localized optical nonlinearity*, IEEE Journal of Selected Topics in Quantum Electronics **11**(2), 2005, pp. 307–312.
[18] JOO-YOUP KIM, JEUNG-MO KANG, TAE-YOUNG KIM, SANG-KOOK HAN, *All-optical multiple logic gates with XOR, NOR, OR, and NAND functions using parallel SOA-MZI structures: Theory and experiment*, Journal of Lightwave Technology **24**(9), 2006, pp. 3392–3399.
[19] YAW-DONG WU, TIEN-TSORNG SHIH, MAO-HSIUNG CHEN, *New all-optical logic gates based on the local nonlinear Mach–Zehnder interferometer*, Optics Express **16**(1), 2008, pp. 248–257.
[20] SANCHIS P., CUESTA-SOTO F., BLASCO J., GARCÍA J., MARTÍNEZ A., MARTI J., RIBOLI F., PAVESI L., *All-optical MZI XOR logic gate based on Si slot waveguides filled by Si-nc embedded in SiO$_2$*, 3rd IEEE International Conference on Group IV Photonics, 2006, pp. 81–83.
[21] BEAUMONT A.R., ATKINS C.G., BOOTH R.C., *Optically induced drift effects in lithium niobate electro-optic waveguide devices operating at a wavelength of 1.51 μm*, Electronics Letters **22**(23), 1986, pp. 1260–1261.
[22] *OptiBPM, Technical Background and Tutorials. Waveguide Optics Modeling Software System*, Version 8.0, Second Edition, Optiwave Inc., 2006.
[23] BARNES C.E., GREENWELL R.A., *Radiation effects in photonic modulator structures*, Proceedings of SPIE **2482**, 1995, p. 48.

[24] ANALUI B., GUCKENBERGER D., KUCHARSKI D., NARASIMHA A., *A fully integrated 20-Gb/s opto-electronic transceiver implemented in a standard 0.13 μm CMOS SOI technology*, IEEE Journal of Solid-State Circuits **41**(12), 2006, pp. 2945–2955.
[25] NORD M., *Optical Switching Technologies for Optical Line, Burst and Packet Switches*, Scientific Report, Telenor Communication, 2002.
[26] WONG K.K., *Properties of Lithium Niobate*, EMIS Datareviews Series No. 28, An INSPEC Publication, 2002, p. 131.
[27] JIN H., BELANGER M., JAKUBCZYK Z., *General analysis of electrodes in integrated-optics and electrooptic devices*, IEEE Journal of Quantum Electronics **27**(2), 1991, pp. 243–251.
[28] BENTINI G.G., BIANCONI M., CERUTTI A., CHIARINI M., PENNESTRI G., SADA C., ARGIOLAS N., BAZZAN M., MAZZOLDI P., *Integrated Mach–Zehnder micro-interferometer on* $LiNbO_3$, Optics and Lasers in Engineering **45**(3), 2007, pp. 368–372.
[29] YARIV A., *Optical Electronics in Modern Communications*, 5th Edition, Oxford University Press, 1996.
[30] SINGH G., BHATTACHARJEE T.P., MUNDRA R., YADAV R.P., JANYANI V., *Design and analysis of the performance of MZI-based all-optical switch exploiting the band gap shifting character of SOA's*, Journal of Optics **38**(1), 2009, pp. 29–37.
[31] CHATTOPADHYAY T., *All-optical programmable Boolean logic unit using semiconductor optical amplifiers on the Mach–Zehnder interferometer arms switch*, IET Optoelectronics **5**(6), 2011, pp. 270–280.
[32] TEKIN T., *Monolithically Integrated Gain Shifted Mach–Zehnder Interferometer for All-Optical Demultiplexing*, PhD Thesis, Faculty of Electrical Engineering and Computer Science, Technical University of Berlin, Germany, 20th July, 2004.

Received June 20, 2011
in revised form January 7, 2012